Fachtagung "Experimentelle Strömungsmechanik"
5.–7. September 2023, München

The formation process of a laminar separation bubble over an SD7003 airfoil at various accelerations

Der Entstehungsprozess einer laminaren Ablöseblase über einem SD7003 Profil bei verschiedenen Beschleunigungen

Wolfgang Dierl, Rainer Hain, Christian J. Kähler
Universität der Bundeswehr München, Werner-Heisenberg-Weg 39, 85577 Neubiberg

Serhiy Yarusevych
University of Waterloo, Waterloo, Ontario N2L 3G1, Canada

Laminar separation bubble, acceleration, boundary layer, vortex shedding
Laminare Ablöseblase. Beschleunigung, Grenzschicht, Wirbelablösung

Abstract

This work examines the influence of acceleration on the formation of a laminar separation bubble. The experiments were performed in a towing tank with an SD7003 airfoil model accelerated from rest to a constant chord Reynolds number. Quantitative flow field measurements were performed using two-component time-resolved Particle Image Velocimetry over a range of accelerations. The aim is to provide insight into the mechanism of LSB formation by a detailed analysis of the spatio-temporal flow development focusing on the LSB formation and dynamics. The associated transient flow development is shown to persist over several convective time scales after steady state free stream velocity is reached, with no significant effect of acceleration on the overall transient duration. However, the acceleration rate has a substantial effect on flow development during the acceleration, with a delayed development of shear layer perturbations observed at lower accelerations.

Introduction

Rapid advancements of applications operating at aerodynamically low Reynolds numbers ($Re_c \leq 500{,}000$), like high-altitude, long-endurance unmanned aerial vehicles and micro air vehicles, continues to pose new research challenges. A defining feature for a lifting surface operating at a low Reynolds number is laminar boundary layer separation on the suction side, which leads to a notable degradation in aerodynamic performance (Lissaman 1983). Following separation, relatively rapid transition to turbulence takes place in the separated shear layer, often leading to mean flow reattachment and the formation of a Laminar Separation Bubble (LSB). The associated flow development and parametric effects of the angle of attack, Reynolds number, and free stream turbulence intensity (Burgmann and Schröder 2008, Ol et al. 2005) have been considered in a number of previous investigations. However, the overwhelming majority of prior studies were conducted under quasi-steady incoming flow conditions. In contrast, the transient flow effects on the LSB have received less attention, despite being encountered in gusty winds or during maneuvering flight. The effect of free-stream acceleration and deceleration between non-zero limiting velocity values was

GALA e.V., Karlsruhe, Germany, ISBN 978-3-9816764-9-5

investigated by (Ellsworth and Mueller 1991). The results show that the LSB response to changes in Reynolds number (Re) differs substantially from the behavior expected from similar quasi-steady changes. Similar observations have been reported in other studies that considered separating flows on lifting surfaces under unsteady effects (e.g. Mancini et al. 2015). The present work experimentally investigates the spatio-temporal formation process of an LSB over an airfoil accelerating from rest, as a model of a vehicle launch.

Experimental setup

All the experiments were performed in a water towing tank at the University of the Bundeswehr Munich. The test facility is 8 m long, with a cross-section of 0.9 × 0.9 m. The water height during the experiments was 0.75 m. An SD7003 airfoil model with a chord length c = 250 mm and a span of 750 mm was employed. To prevent distortions from a wavy water surface and mitigate end effects, a glass end plate was installed (Figure 1a).

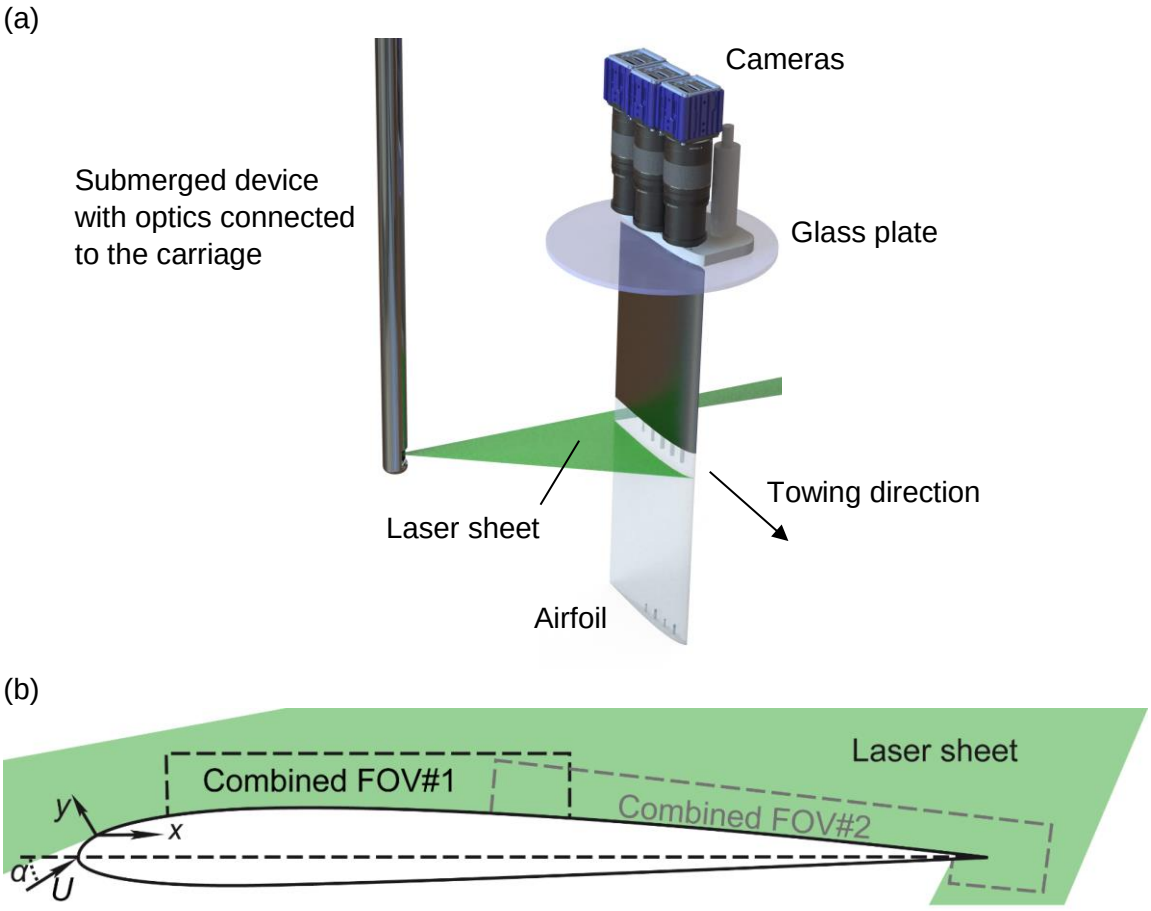

Figure 1: Experimental setup (a) airfoil model and PIV arrangement (b) Fields of View (FOV) and coordinate system definition.

The model was mounted at an angle of attack α = 6° and was accelerated from rest to a constant chord Reynolds number Re_c = 60,000. Four different accelerations a were considered and the corresponding nondimensional acceleration parameters ($A_C = ac/(U_{final})^2$, where U_{final} is the final, steady-state velocity) are listed in Table 1.

GALA e.V., Karlsruhe, Germany, ISBN 978-3-9816764-9-5

Table 1: Acceleration cases

Case	A	B	C	D
A_c	0,22	0,43	0,87	2,17

Additionally for Case C, a Re_c of 30,000 (Case C_{30}) and 45,000 (Case C_{45}) were considered.

Quantitative flow field measurements were performed using two-component time-resolved Particle Image Velocimetry (PIV) in a setup illustrated in Figure 1b. The water in the tank was seeded with 10 µm hollow glass spheres from LaVision, with a specific gravity of 1.1. The flow was illuminated by a Photonics DM150-532 DH Nd:YAG double pulse laser. The laser sheet was formed within a submerged device connected to the carriage of the towing tank, containing a combination of spherical and cylindrical lenses. Particle images were acquired by three cameras (LaVision Imager sCMOS) at 55 Hz in double frame mode (42 Hz and 30 Hz for Re_c = 45,000 and Re_c = 30,000, respectively). Each camera was equipped with a Zeiss Makro Planar 100 mm fixed focal-length lens set to a numerical aperture of 4. The camera sensors were cropped to 2560 px × 967 px each. The combined field of view (FOV) at measurement position #1 and #2 (Figure 1b) from all three cameras was 18 × 145 mm², with a magnification factor of 0.31. To compute the vector field a sequential cross-correlation function, with a final interrogation window size of 24 px × 24 px and an overlap of 75 % was used. This results in a vector pitch of 0.13 mm for FOV #1 and #2.

A magnet band sensor (MBS) from Waycon was used to measure the position of the carriage. The MBS data were recorded at 100 kHz simultaneously with the Q-switch signal from the laser, allowing to establish the correspondence between the measured airfoil motion and velocity fields.

Ten independent test runs, each yielding 400 measured velocity fields, were conducted per case. The distance travelled over which velocity measurements were conducted for each run was 3.25 m (or 13·c). PIV measurements were first performed for FOV #1, and the runs were repeated to facilitate measurements in FOV #2 (Figure 1).

Preliminary PIV measurements of the water movement subsequent to a measurement run were conducted. The time separation between each run was set to at least 300 s to reduce any adverse influence of residual perturbations from the previous run. Figure 2 illustrates the mean water movement velocity v_m and turbulence intensity level Tu_{240} in the towing tank based on a reference velocity v_{ref} = 240 mm/s. After 300 s v_m dropped below 1.2 % of v_{ref} and Tu_{240} below 0.05 %.

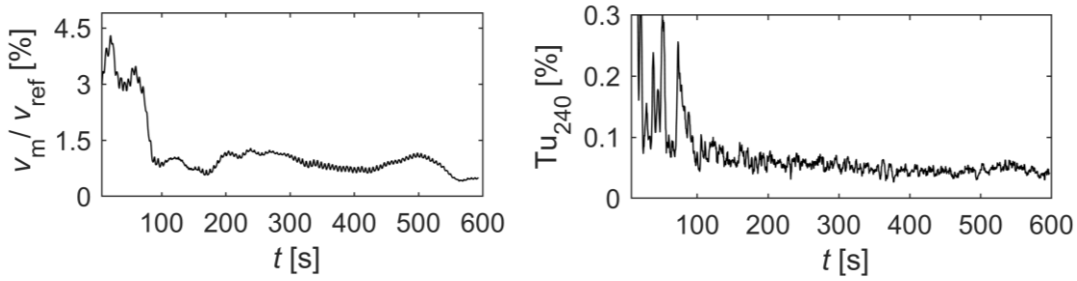

Figure 2: Normalized mean flow velocity and turbulence level within towing tank subsequent to a measurement run.

GALA e.V., Karlsruhe, Germany, ISBN 978-3-9816764-9-5

Results

The formation of a LSB is depicted for case C (Table 1). Figure 3 presents the overall formation process of the LSB on the suction side of the airfoil using the local wall parallel velocity component. The sequence of consecutive times frames is spaced by 16/55 s, with the first frame corresponding to t = 1.73 s from the onset of airfoil motion. At this time the acceleration phase is already finished and the model moves at a constant speed. The formation process can be divided into three phases. First, a laminar boundary layer forms over the complete wing, followed by the second phase, a simultaneous vortex formation in the area of the second half of the airfoil and the continuous movement of the shear layer roll-up point towards the leading edge. Finally the third phase in which the roll-up point stabilizes and the laminar separation bubble maintains its typical topology for the selected configuration.

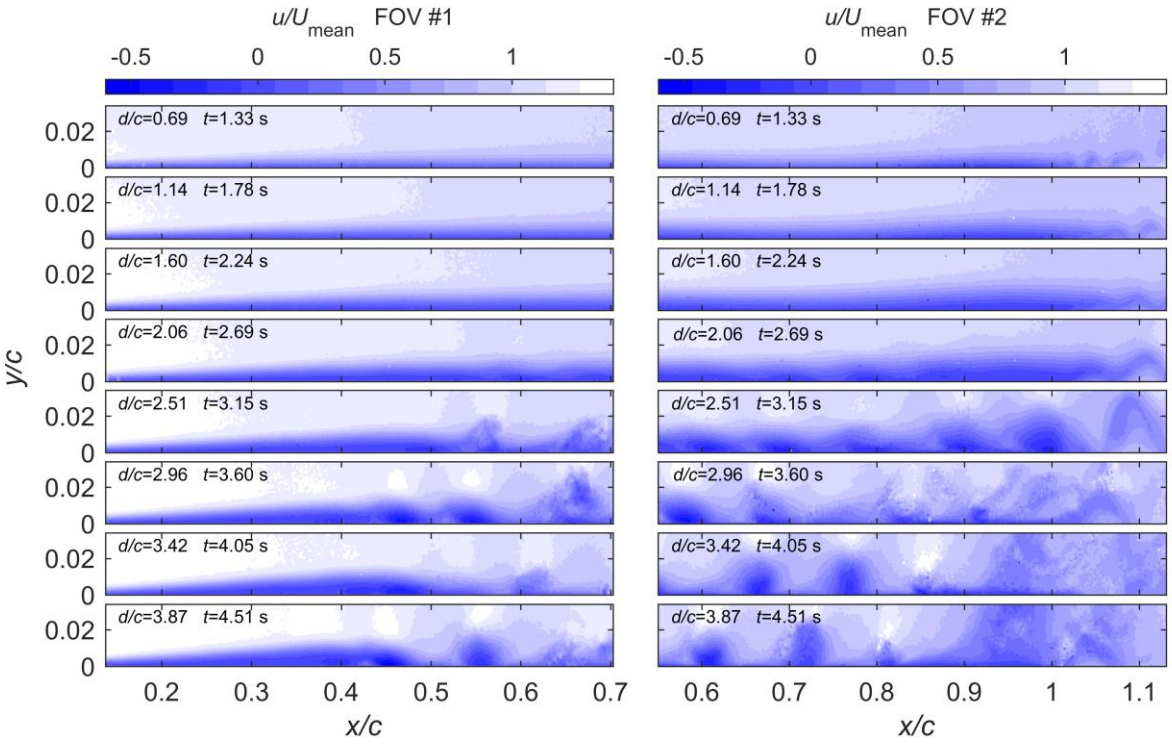

Figure 3: Formation process of the LSB for case C illustrated using non dimensional wall parallel velocity component.

Figure 4 offers another perspective on the spatio-temporal flow development. It presents contours of local boundary layer displacement thickness (δ^*) computed based on the integration of the wall-tangent velocity component over the vertical extent of the field of view, with the local instantaneous edge velocity taken as the reference. The results are plotted versus the relative distance traveled by the wing (d/c) with final velocity reached at end of the acceleration phase, indicated by the black dotted line. It can be seen that acceleration from rest results in significant changes in the flow. Furthermore it is evident that it takes several convective time scales to reach quasi-steady state after the final wing velocity is reached. In particular, a continuous growth of δ^* with respect to d/c can be seen at all x/c locations, saturating at approximately d/c = 8 at a position of x/c = 0.34 and at d/c = 11 at a position of x/c = 0.38 for a Reynolds number of 60,000 and 45,000, respectively. The measuring distance of 13·c is not sufficient to reach quasi-steady state for Re = 30,000. Comparing the results of these three Re reveals, as expected, that δ^* and d/c are inversely proportional to Re.

GALA e.V., Karlsruhe, Germany, ISBN 978-3-9816764-9-5

Based on a moving window average over 30 frames, an estimate of separation and reattachment locations is provided by the solid and dashed lines, respectively. They show an upstream movement of an LSB, which moves into FOV#1 at $d/c \approx 2.4$, which is in between frame four and five in Figure 3. The associated periodic shedding of shear layer structures is reflected in periodic fluctuations in the computed δ^* in Figure 4.

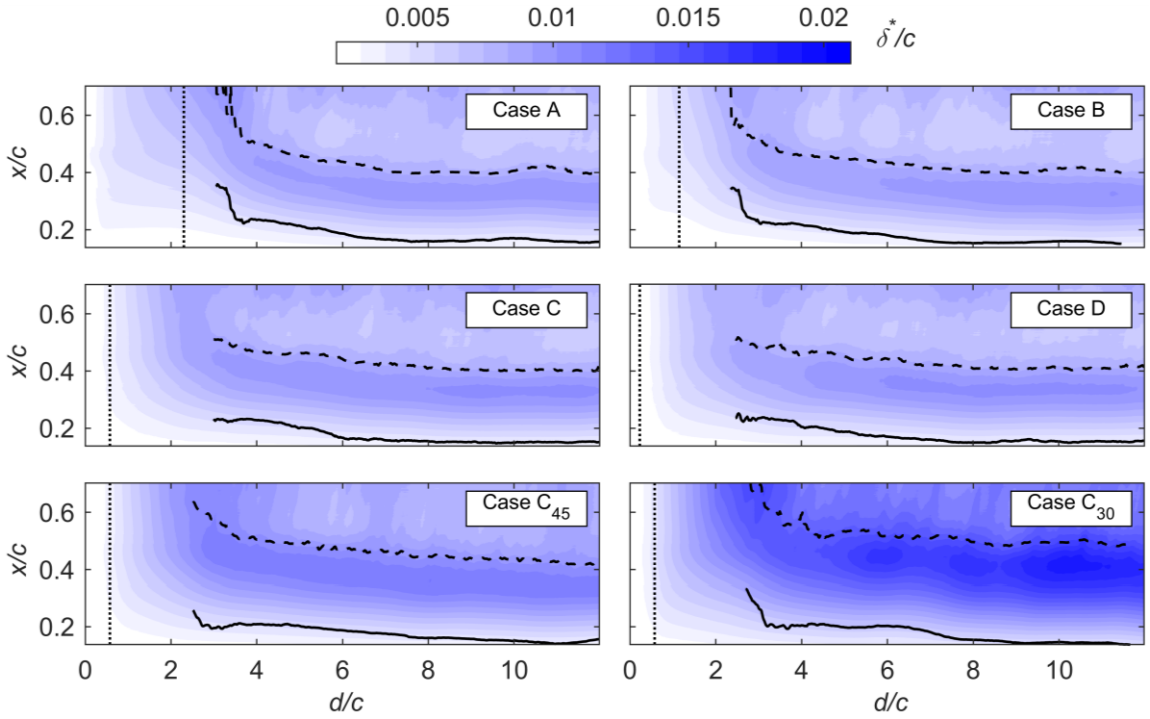

Figure 4: Spatio-temporal evolution of displacement thickness for all cases in FOV#1. Thick solid and dashed black lines mark window-averaged locations of separation and reattachment, respectively. Black dotted line represents end of acceleration phase.

The effect of flow acceleration is explored in Figure 5, which presents δ* computed at three locations for all the accelerations and Re investigated. The chosen chord positions in Figure 5 are located at the separation point, the point of maximum bubble height and at the reattachment point of the LSB in steady state conditions for a constant Re. While notable differences are observed at the earlier stages of flow development, the results indicate that significant changes take place in the flow field after the acceleration phase, and the overall transient takes approximately eight convective times for all accelerations investigated. This agrees with the transient durations for an LSB due to changes in controlled perturbation (Yarusevych and Kotsonis 2017), suggesting that the transient dynamics is driven by that of the LSB in the cases considered here. At the earlier stages of flow development, cases C and D show a continuous growth in δ^* with subsequent saturation to a steady-state value. In contrast, an intermediate plateau is reached in δ^* for case A and B during the second half of the acceleration phase, and continuous growth in displacement thickness is reestablished when the final wing velocity is reached. A detailed analysis of the results reveals that the observed differences in the flow development during the initial phase of acceleration are related to the differences in the onset and early development of shear layer perturbations. In particular, a delayed development of shear layer perturbations is observed at lower accelerations. This and the subsequent differences in the shear layer development can be expected for the relatively height values of the acceleration parameter considered here, $K = (\nu/U(x)^2)\times(\mathrm{d}U(x)/\mathrm{d}x) > 3.6\times10^{-6}$, where $U(x)$ is the local free stream velocity and ν the kinematic viscosity (Bourassa and Thomas 2009).

GALA e.V., Karlsruhe, Germany, ISBN 978-3-9816764-9-5

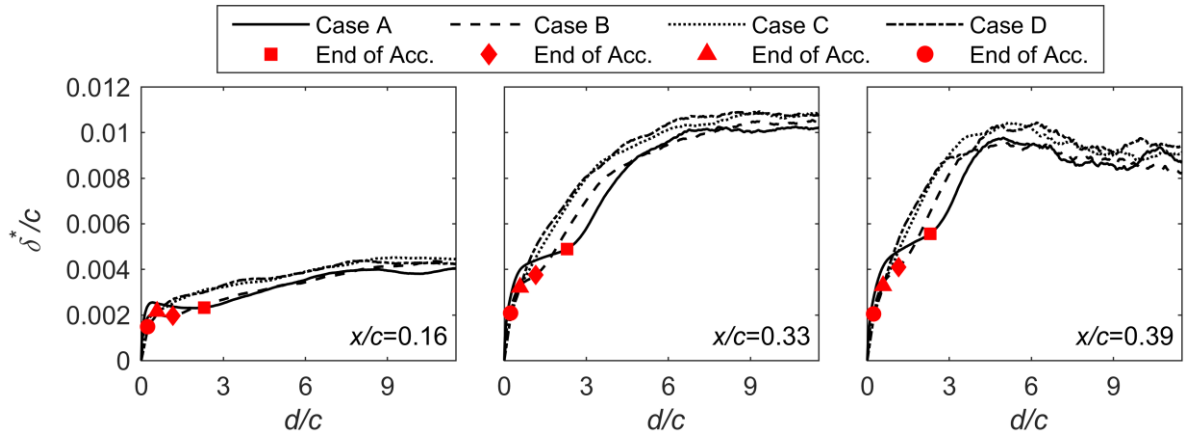

Figure 5: Variation of displacement thickness computed at three chord positions.

To evaluate the initial formation process of the vorticies over the airfoil in detail, Figure 6 illustrates the onset of vortex formation over the airfoil by a sequence of consecutive time frames, spaced by 8/55 s, with the first frame corresponding to t = 2.64 s from the onset of airfoil motion. The results reveal the appearance of periodic undulations in the shear layer that develop into distinct periodic shedding of vortices at later times, similar to the Kelvin-Helmholtz instability driven vortex shedding in a quasi-steady LSB (e.g., Wattmuff 1999). However, low amplitude perturbations that can be inferred from the waviness of the shear layer in the first flow field of the sequence appear to grow both in space and time. The distinct convective amplification can be seen by tracing the same structures in subsequent images, some of which are connected by dashed lines in Figure 6. Also, a notable increase in perturbation amplitude can be observed at a given x/c location, for example at x/c = 0.6. This may indicate that the initial stage of transition may be governed by a combination of convective and global instability mechanisms. Progressively, the convective instability mechanism appears to take over, and a typical spatial amplification of structures is observed in the last frames of the sequence.

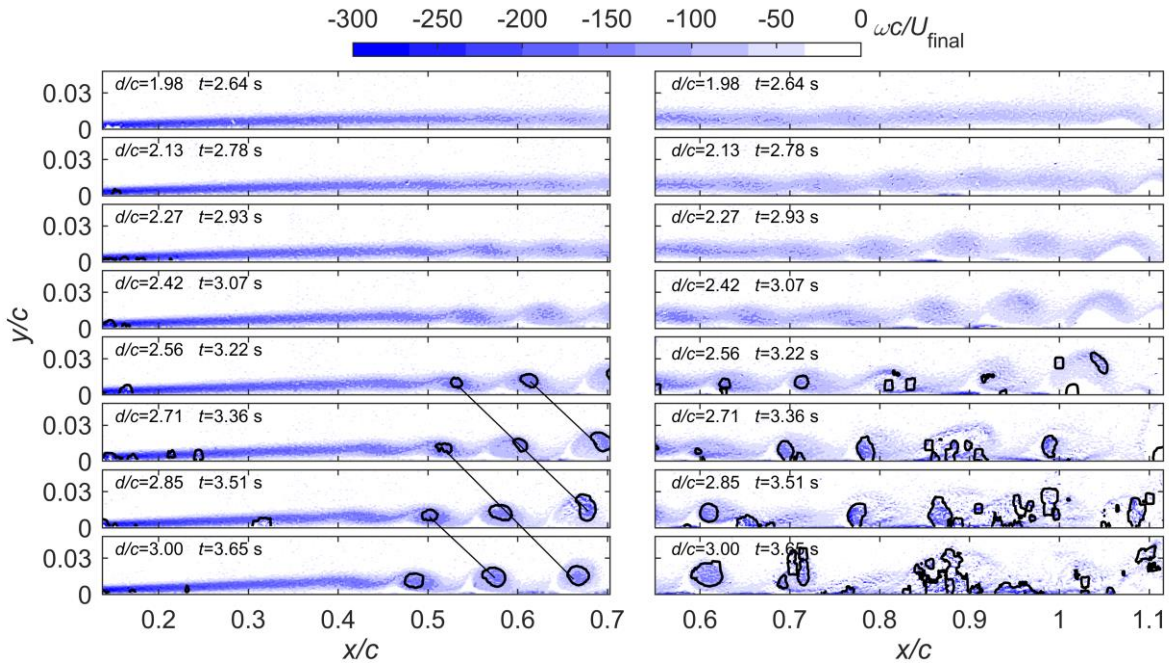

Figure 6: Onset of vortex formation for case C illustrated using spanwise vorticity contours ω. Solid black line contours correspond to $\lambda_2 = -80$ to identify.

GALA e.V., Karlsruhe, Germany, ISBN 978-3-9816764-9-5

It can also be inferred from the last four frames that the shear layer roll-up location progressively moves upstream, with an estimated rate of $0.14c\ s^{-1}$. The estimated drift velocity of the vortices from the later part of the flow field sequence in Figure 6 is $U_{drift} = 0.59 \cdot U_{final}$, which agrees well with $U_{drift} = 0.65 \cdot U_{final}$ determined by Pauley et al. 1990.

Based on a wavelet and Fourier analysis of wall-normal velocity fluctuations shown in Figure 7, the vortex shedding frequency is $f_s = 6$ Hz, $St = f_s c/U_{final} = 6$. Despite the upstream movement of the roll-up location, the shedding frequency remains relatively constant from the onset of distinct shedding and 6 Hz matches that measured in a quasi-steady LSB established at $U_{final} = 0.25$ m/s ($Re_c = 60{,}000$, AoA = 6°). The estimated shedding frequency is in general agreement with the parametric correlation provided in (Boutilier and Yarusevych 2012), but is lower than that measured by Burgmann and Schröder 2008 on the same airfoil at matching operating conditions. The latter can be attributed to a notably higher level of background perturbations in the latter reference, which also results in a smaller LSB.

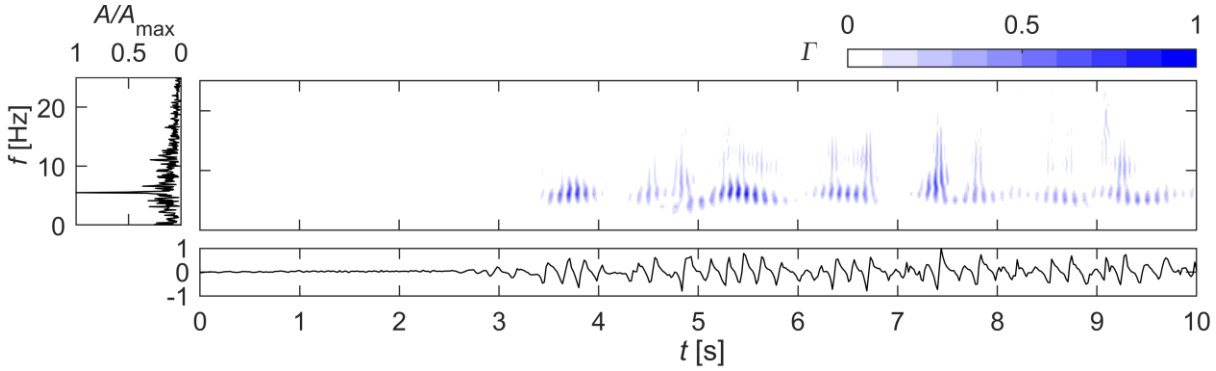

Figure 7: Normalized wavelet coefficient (Γ) contours from wall normal velocity fluctuation. Extracted normalized fluctuation signal shown on the bottom with corresponding Fourier analysis on the left.

Conclusion

The present study examined the influence of various accelerations on the formation process of a laminar separation bubble. The formation process consists of three phases, whereby for the configurations investigated, the influence of acceleration can only be seen during the first phase. The detailed analysis of the initial formation process of the vorticies during phase two may indicate that the initial stage of transition may be governed by a combination of convective and global instability mechanisms. A wavelet analysis of the vortex shedding frequency revealed, that it remains relatively constant from the onset of shedding to reaching quasi-steady conditions at the final chord Renyolds number.

Acknowledgement

The authors gratefully acknowledge the financial support of the German Research Foundation for this project (Analysis of the transition process around laminar separation bubbles (LSB‘s) in a towing tank using time-resolved 3D particle tracking techniques, Project number 422177304).

GALA e.V., Karlsruhe, Germany, ISBN 978-3-9816764-9-5

References

Bourassa, C., Thomas, F.C., 2009: “An experimental investigation of a highly accelerated turbulent boundary layer”, Journal of Fluid Mechanics, 634, pp. 359–404

Boutilier, M.S.H., Yarusevych, S., 2012: “Parametric study of separation and transition characteristics over an airfoil at low Reynolds numbers”, Experiments in Fluids, 52(6), pp 1491–1506.

Burgmann, S., Schröder, W., 2008: “Investigation of the vortex induced unsteadiness of a separation bubble via time-resolved and scanning PIV measurements”, Experiments in Fluids, 45(4), pp. 675–691

Ellsworth, R.H., Mueller, T.J., 1991: “Airfoil boundary layer measurements at low Re in an accelerating flow from a nonzero velocity”, Experiments in Fluids, 11(6), pp. 368–374

Lissaman, P.B.S., 1983: “Low-Reynolds-Number Airfoils”, Annual Review of Fluid Mechanics, 15(1), pp. 223–239

Mancini, P., Manar, F., Granlund, K., Ol, M.V., Jones, A.R., 2015: “Unsteady aerodynamic characteristics of a translating rigid wing at low Reynolds number”, Physics of Fluids, 27(12), 123102

Ol, M.V., McCauliffe, B.R., Hanff, E.S., Scholz, U., Kähler, C.J., 2005: “Comparison of Laminar Separation Bubble Measurements on a Low Reynolds Number Airfoil in Three Facilities”, AIAA Paper, 5149

Pauley, L.L., Moin, P., Reynolds, W.C., 1990: “The structure of two-dimensional separation”, Journal of Fluid Mechanics, 220, pp. 397–411

Wattmuff, J.H., 1999: “Evolution of a wave packet into vortex loops in a laminar separation bubble”, Journal of Fluid Mechanics, 397, pp. 119–169

Yarusevych, S., Kotsonis, M., 2017: “Steady and transient response of a laminar separation bubble to controlled disturbances”, Journal of Fluid Mechanics, 813, pp. 955–990

GALA e.V., Karlsruhe, Germany, ISBN 978-3-9816764-9-5